cm CHEMISTRY OF MATERIALS

JULY 22, 2014 | VOLUME 26 | NUMBER 14 | pubs.acs.org/cm

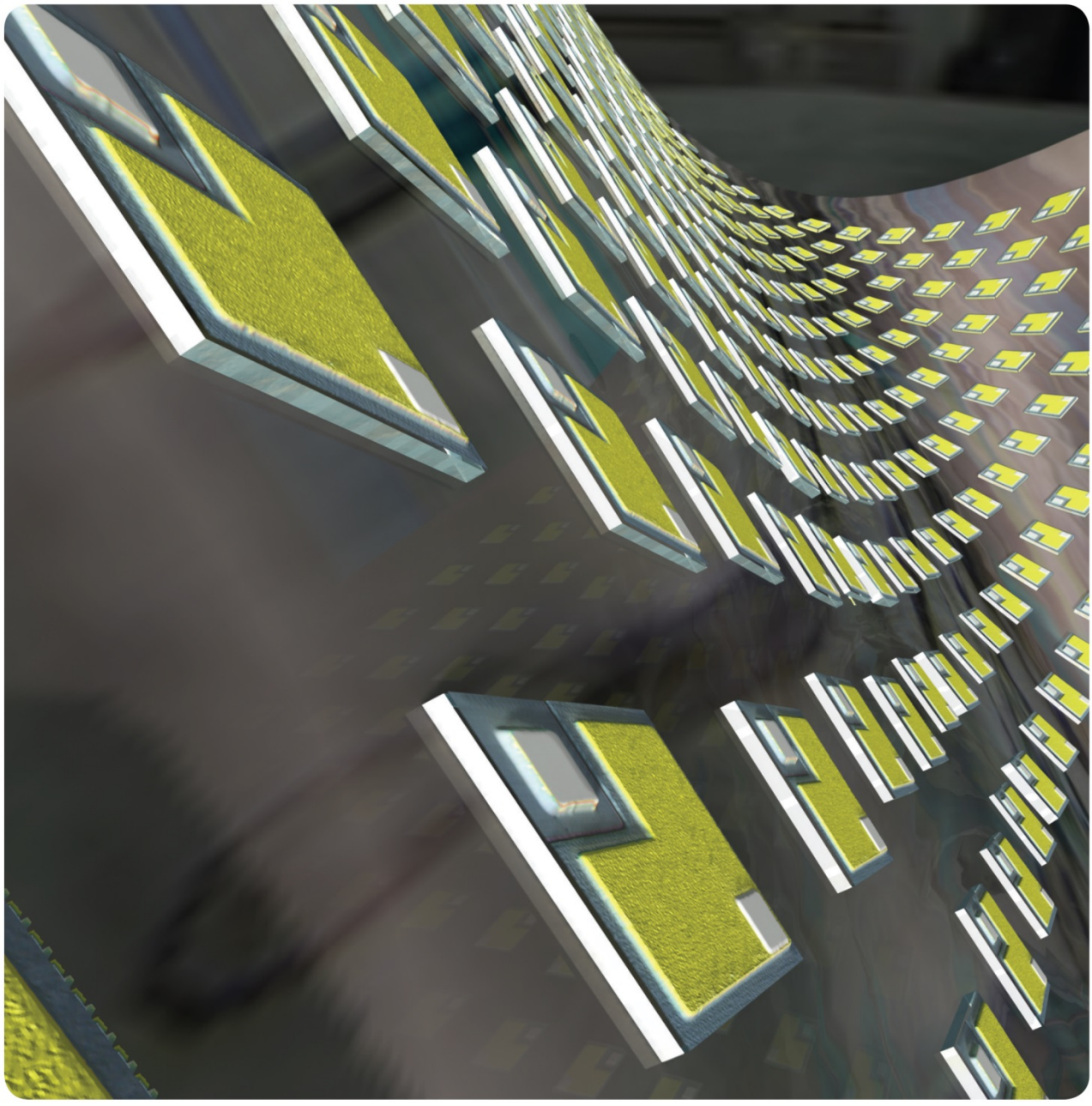

ACS Publications
Most Trusted. Most Cited. Most Read.

www.acs.org

CHEMISTRY OF MATERIALS

Article

pubs.acs.org/cm

Thin Film Receiver Materials for Deterministic Assembly by Transfer Printing

Tae-il Kim,*[,†] Mo Joon Kim,[‡] Yei Hwan Jung,[§] Hyejin Jang,[†] Canan Dagdeviren,[∥] Hsuan An Pao,[∥] Sang June Cho,[§] Andrew Carlson,[∥] Ki Jun Yu,[⊥] Abid Ameen,[∥] Hyun-joong Chung,[△] Sung Hun Jin,[∥] Zhenqiang Ma,[§] and John A. Rogers*[,∥,⊥,#]

[†]Center for Neuroscience Imaging Research (CNIR), Institute of Basic Science (IBS), School of Chemical Engineering, Sungkyunkwan University (SKKU), Suwon 440-746, Korea

[‡]R&I Korea, Solvay Special Chemicals, Solvay Korea Co. LTD, Seoul 120-750, Korea

[§]Department of Electrical and Computer Engineering and , University of Wisconsin—Madison, Madison, Wisconsin 53706, United States

[∥]Department of Materials Science and Engineering, [⊥]Department of Electrical Computer and Engineering, and [#]Chemistry, Mechanical Science and Engineering, Beckman Institute for Advanced Science and Technology, Frederick Seitz Materials Research Laboratory, University of Illinois at Urbana−Champaign, Urbana, Illinois 61801, United States

[△]Department of Chemical and Materials Engineering, University of Alberta, Edmonton, Alberta T6G 2V4, Canada

Supporting Information

ABSTRACT: We present a specially designed materials chemistry that provides ultrathin adhesive layers with persistent tacky surfaces in solid, nonflowable forms for use in transfer printing and related approaches to materials and micro/nanostructure assembly. The material can be photocured after assembly, to yield a robust and highly transparent coating that is also thermally and electrically stable, for applications in electronics, optoelectronics, and other areas of interest.

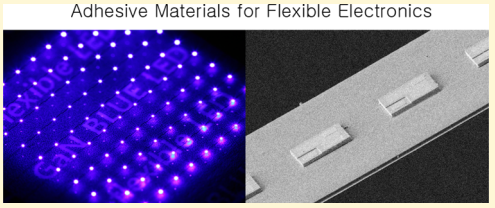

Advanced electronic materials and printing processes have enabled rapid advances in functional capabilities for flexible electronics,[1−6] biointegrated devices,[7−9] and other types of emerging systems. A high speed, deterministic method for assembly, sometimes known as transfer printing, has become popular in these and related fields due to its ability to heterogeneously integrate multiple types micro/nanoscale materials in sparse or dense coverages, over large or small areas, in two- or three-dimensional layouts, on nearly any class of substrate.[1,10−13] Recently reported schemes using automated tools show promise not only for research but also for practical, high-volume manufacturing.[13,14] Although the process can be conducted in a mode that does not require separate adhesives to guide the transfer,[10,12,13,15−17] general uses typically benefit from surface chemistries that enable strong bonding between the assembled materials and the underlying substrate.[18−20] An ideal adhesive for this purpose would avoid extensive chemical modification of surfaces or physical flow of materials and would offer rapid bonding without the need for special preparations, thermal processing, or ultraviolet illumination. In addition, the surface chemistry would persist to enable processing in a repetitive sequence of steps (i.e., step-and-repeat printing).[18−20] Conventional adhesive materials can provide attractive features for many applications, but they do not simultaneously satisfy the requirements listed above. Here, we present a specially designed chemistry that enables implementation as ultrathin films (∼150 nm) with persistent tacky surfaces (degradation time is more than 2 weeks), in solid, nonflowable forms. The material can be photocured after assembly, to yield a robust and highly transparent (∼99 % at 550 nm) coating that is also thermally and electrically stable, for applications in electronics, optoelectronics, and other areas of interest. This material significantly enhances device and substrate options in transfer printing.[8,21,22] The results presented in the following highlight the chemical and mechanical properties and include demonstrations of various devices formed by transfer printing with inorganic semiconductor materials.

Figure 1 outlines the procedures for transfer printing with this type of adhesive, along with its chemical components. Figure 1A,B show dense arrays of material microstructures formed on a source wafer (A) and then transferred into sparse layouts on a different substrate (B) using a stamp (shown here with just one relief post, for simplicity). The role of the adhesive is to ensure stronger bonding to the substrate than to the stamp, during the transfer step. Figure 1C,D shows an example of InGaN/GaN microscale inorganic light-emitting diodes (μ-ILEDs, formed as complete devices on a sapphire growth substrate, each with lateral dimensions: 100 × 100 μm^2; thicknesses, 6.45 μm; and separations, 20 μm). Here, laser lift off allows release of these μ-ILEDs onto a substrate from which

Received: March 21, 2014
Revised: May 18, 2014
Published: May 30, 2014

   dx.doi.org/10.1021/cm501002b | Chem. Mater. 2014, 26, 3502−3507

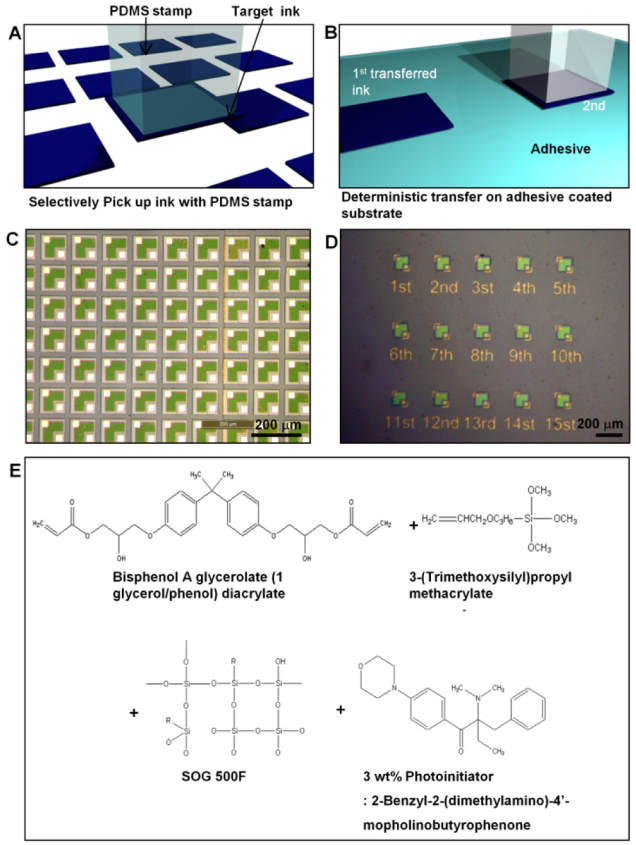

Figure 1. Schematic illustrations of deterministic microstructure assembly by transfer printing onto a substrate coated with a thin adhesive layer. (A) Releasable material structures fabricated on a mother wafer, prepared to allow retrieval onto the surface of a stamp. (B) Transfer printing delivers sparse array of material structures onto a target substrate coated with a thin adhesive. (C) Arrays of μ-ILEDs (100 × 100 μm^2 separated by 20 μm) fabricated on a sapphire substrate, including *L*-shaped current spreading p-contacts (Ni:15 nm/Au:15 nm) and square (25 × 25 μm^2) n- and p-contact pads (Cr: 15 nm/Au:300 nm). (D) Formation of arrays of μ-ILEDs with 200 μm *x*- and 400 μm *y*-spacings, in a mode in which one device was printed per day. (E) The adhesive is composed of Bisphenol A glycerolate (1 glycerol/phenol) diacrylate (acrylic monomer, Sigma-Aldrich), 3-(trimethoxysilyl) propyl methacrylate (acrylic monomer, 98%, Sigma-Aldrich), Spin-on-Glass (SOG 500F, Filmtronics Inc.), polymerization initiator; 2-benzyl-2-(dimethylamino)-4′-mopholinobutyrophenone (97%, Sigma-Aldrich), and anhydrous ethanol (Sigma-Aldrich) with 200:100:100:9:1700 weight ratio, respectively.

they can be retrieved by a stamp for printing.[21] Figure 1D, which illustrates their deterministic assembly into arrays with spacings of 200 and 400 μm along the *x* and *y* axes, respectively, also demonstrates the persistent nature of the surface of the adhesive. In this set of experiments, one μ-ILED was printed per day for 15 consecutive days. The transfer yields remained constant over this entire time period.

The chemical composition of the adhesive is critically important. Figure 1E summarizes the different components: bisphenol A glycerolate (1 glycerol/phenol) diacrylate (acrylic monomer, Sigma-Aldrich), 3-(trimethoxysilyl) propyl methacrylate (acrylic monomer, 98%, Sigma-Aldrich), Spin-on-Glass (SOG 500F, Filmtronics Inc.), polymerization initiator; 2-benzyl-2-(dimethylamino)-4′-mopholinobutyrophenone (97%, Sigma-Aldrich), and anhydrous ethanol (Sigma-Aldrich). Mixing these materials in a weight ratio of 200:100:100:9:1700 yields the formulation used here; other ratios are possible. Bisphenol A glycerolate is responsible for creating a surface that is sufficiently tacky to allow high yield release of the devices from the stamp (formed using poly(dimethylsiloxane), PDMS), due to its acrylate functional groups and their unshared π-electrons. The SOG provides a hydrophilic surface that also improves the thermal resistance and hardness after thermal curing. 3-(Trimethoxysilyl) propyl methacrylate offers bifunctional acrylate and alkoxy groups, to serve as a cross-linker between bisphenol A glycerolate and SOG. The alkoxy groups of the silane (3-(trimethoxysilyl) propyl methacrylate) react with H_2O to yield silanol groups (−SiOH) that are capable of reacting with the hydroxyl groups of the SOG. The acrylate groups of the SOG can also react with the acrylate groups of bisphenol A glycerolate by ultraviolet (UV) curing in the presence of a radical initiator (2-benzyl-2-(dimethylamino)-4′-mopholinobutyrophenone). Anhydrous ethanol can dissolve these components homogeneously, for well-controlled behavior in spin-casting. These components have the additional feature that they are each transparent throughout the visible range.

Substrate preparation for materials such as polyethylene terephthalate (PET) and glass involves washing with isopropyl alcohol and acetone followed by drying under a stream of nitrogen. Spin coating (e.g., 2000−3000 rpm with 15 wt % solution in EtOH) and thermal annealing (~10 min at 110 °C on a hot plate) yields a 150 nm thick adhesive film. After transfer printing using a PDMS stamp, UV flood exposure (2 min exposure, ~100 mJ/cm^2 dose) initiates polymerization and yields permanent bonds to form a solid film with a tacky surface.

Figure 2 shows FT-IR (Fourier transform infrared spectroscopy) spectra of an as-coated (without baking; black line), annealed (~10 min at 110 °C on a hot plate; red line), and photocured (UV flood exposure for 2 min; blue line) adhesive

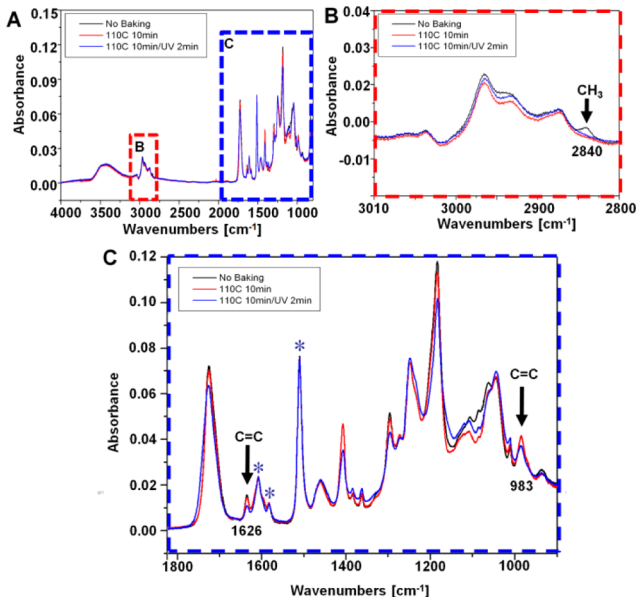

Figure 2. FTIR spectra of a spin-cast layer of adhesive without annealing (black), with annealing (red), and UV cured with annealing (blue). (A) Broad range spectrum, from 4000 to 500 cm^{-1}. (B−C) Enlarged spectra for regimes from 3010 to 2800 cm^{-1} and from 1830 to 900 cm^{-1} highlighted in red and blue dashes, respectively.

dx.doi.org/10.1021/cm501002b | *Chem. Mater.* 2014, 26, 3502−3507

film. Figure 2A shows spectra from 4000 cm^{-1} wavenumbers to 500 cm^{-1}. The wide band at 3443 cm^{-1} arises from the hydroxyl groups. Figure 2B,C are enlarged images of the red and blue dashed regions of Figure 2A, respectively. The results indicate that acrylate polymerization (shown in C) and annealing induces chemical bonding (shown in B) between the 3-(trimethoxysilyl) propyl methacrylate component and the hydroxyl surface functionality created by oxygen plasma treatment of substrate such as PET film or glass. The CH_3− terminal group of the 3-(trimethoxysilyl) propyl methacrylate occurs at ∼2840 cm^{-1}. Photoinitiation generates enough radicals to induce acrylate polymerization; the consequence is that the C═C bonds, which appear at 1626 and 983 cm^{-1}, convert to C—C bonds. Ester carboxyl groups are observed at 1725 and 1187 cm^{-1}. The C═C bonds associated with the aromatic rings (*; 1606, 1580, and 1506 cm^{-1}) do not change during this process.

Even after 7 days at room temperature in the dark, there are no significant changes in the chemistry, as evidenced by the FTIR results, Figure 3A. Measurements of adhesion force

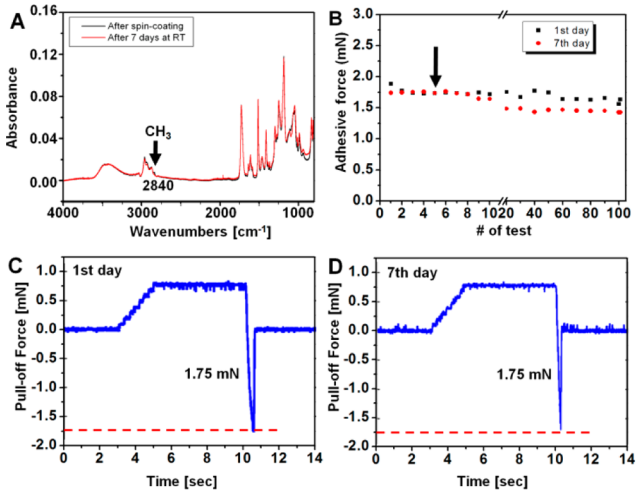

Figure 3. (A) FTIR spectra immediately after spin-casting (black) and after 7 days (red) at room temperature without UV exposure. (B) Adhesion tests for 100 cycles. The results highlighted by the black arrow in (B) are shown in (C) immediately after spin-casting and in (D) after 7 days.

appear in Figure 3B−D. Here, an automated tool first establishes contact between a stamp and a silicon wafer coated with the adhesive at an approach rate of 5 μm/s until reaching a compressive preload force of 500 μN. After a dwell time of 4 s, the stage retracts the stamp at a rate of 100 μm/s, in a manner similar to that reported previously.[16] From the resulting force−displacement curves recorded by a load cell, a maximum pull-off force can be determined. Results of repeated measurements (100 times), at several locations on the silicon mounted adhesive layer, appear in Figure 3B. The data support the sustained adhesive capability of the polymer and also reveal the extent of spatial differences in the adhesive character. Figure 3C,D compares adhesive forces between results (black arrow) obtained using a freshly spin-coated adhesive (black dots) and one after 7 days (red dots). The adhesive forces, ∼1.75 mN, are almost identical.

Figure 4 summarizes the optical, thermal, and dielectric properties. The transmittance of a 150 nm thick film measured by a UV−vis spectrometer (PerkinElmer Inc.) is ∼99% (blue

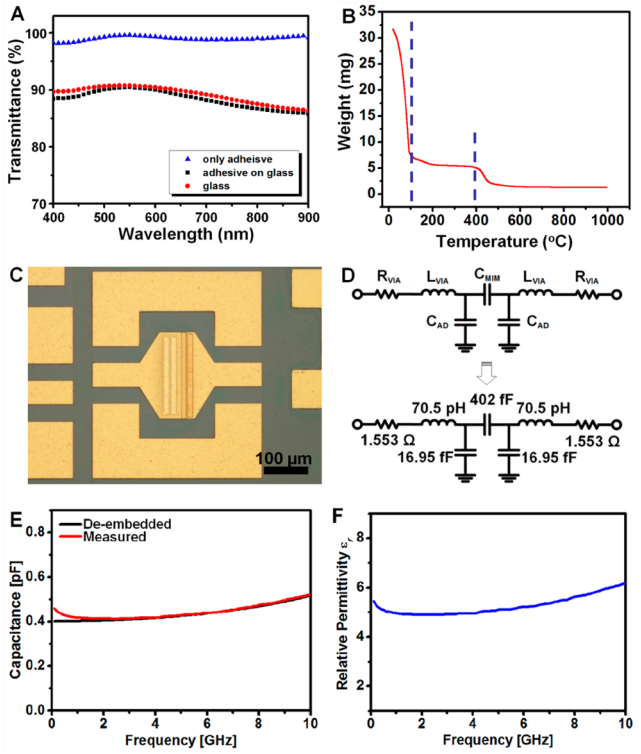

Figure 4. Optical, thermal, and dielectric properties. (A) Optical transmittance (%) as a function of wavelength. Black, red, and blue lines show (B) thermogravimetric data and (C) optical micrograph of a MIM capacitor with Au electrodes and adhesive dielectric. (D) Equivalent circuit model and its de-embedded circuit. The lumped elements are matched and de-embedded from measured S-parameters of the capacitor using ADS. (E) Capacitance as a function of frequency. De-embedded and measured results are shown in black and red lines, respectively. (F) Measured relative permittivity (ε_r) of the adhesive as a function of frequency. Linear range of ε_r between 5 and 6 is observed in the 0 to 10 GHz frequency range.

dots) in the visible range. Transmittance comparisons between glass (red dots) and adhesive coated glass (black dots) are also shown. Figure 4B presents data from thermal gravimetric analysis (TGA, Q50; TA Instruments). Temperatures approaching 100 °C show results consistent with the onset of solvent (EtOH) evolution. The material pyrolyzes at ∼400 °C. The absence of weight change from 100 to 400 °C is consistent with excellent thermal stability.

Figure 4C−F shows the dielectric properties measured in the radio frequency (RF) range using a simple metal−insulator−metal (MIM) capacitor (40 × 200 μm), as shown in Figure 4C. Extraction from scattering (S) parameters measured using a network analyzer (Agilent E8364A) involves de-embedding values from equivalent circuits optimized using Agilent Advanced Design System (ADS) software. Figure 4D shows the lumped element circuit model consisting of the MIM capacitor (C_{MIM}), parasitic substrate capacitance (C_{AD}), series resistances (R_{VIA}) to capture dielectric losses, and the lead inductances (L_{VIA}). The simulated result yields good agreement with measurement, as shown in Figure 4E. A simple parallel plate model,

$$C_{MIM} = \frac{\varepsilon_0 \varepsilon_r A}{t}$$

dx.doi.org/10.1021/cm501002b | Chem. Mater. 2014, 26, 3502−3507

where $\varepsilon_0 = 8.8542 \times 10^{-12}$ F·m^{-1}, enables extraction of the relative permittivity (ε_r). Figure 4F shows that the ε_r is ∼5 in frequencies between 0 and 10 GHz. This value is relatively high compared to that of most polymer alternatives, which have typical values that range between 2 and 3. We note that the constituent materials include aromatic functional groups, inorganic components, and their polymerization and yield relatively high dielectric permittivities, e.g., SOG (3.0−3.9 at 1 MHz)[23] and bisphenol A glycerolate diacrylate monomer (∼11 at 1 MHz).[24] The relatively high dielectric constants suggest potential for use in RF devices.

Examples of uses of the adhesive in transfer printing for flexible electronics appear in Figure 5 and include InGaN μ-ILEDs (shown in A), ZnO ribbons for mechanical energy harvesting (B), printed silicon photovoltaic microcells (C), silicon membranes (D), and GaAs chips (E). Figure 5A shows several μ-ILEDs and an array of 100 on a flexible PET substrate (left) and glass (right). The graph on the right shows current−voltage characteristics recorded from the full 10 × 10 array; the inset shows an image, illustrating defect free operation. Figure 5B presents an image of an array of ZnO ribbons on a polyimide substrate, after processing to form capacitor-type thin film harvesters. Here, the ZnO (500 nm) lies between bottom (200 nm) and top electrodes (200 nm) of Au that define an active area of 100 μm × 2.02 mm. A complete harvester consists of six groups of devices; each group includes 10 individual capacitor structures electrically connected in parallel. Figure 5C shows a tilted scanning electron micrograph of two printed bars of silicon (left) and their use in photovoltaic cells (inset), with current−voltage responses under illumination (right). The individual cells have a length of 1.55 mm, a width of 50 μm, and thickness of ∼15 μm. The right graph for Figure 5C shows the measured current density as a function of voltage for a single cell. The efficiency and the fill factors, without any light trapping schemes, are 6.2% and 71%, respectively. The inset illustrates an array of cells. Figure 5D,E shows a 300 nm thick single crystal silicon nanomembrane on glass and an array of GaAs plates on PET.

The materials presented in this study provide a nearly ideal set of characteristics for use with transfer printing and similar techniques for assembly of solid materials or device structures. These and related chemistries have promise for further extending the reach of these methods.

EXPERIMENTAL SECTION

Measurement of Adhesive Force. A custom setup consisting of a precision load cell (GSO-10, Transducer Techniques) supported on a manual tip/tilt platform and attached to automated *x*-, *y*-translational stages allowed precision measurement of adhesive force. An independent vertical translational stage (Aerotech PRO 165) coupled with a rotation platform enabled contact between the rectangular PDMS stamp (5:1 monomer:curing agent, 100 μm × 100 μm × 100 μm) and a target substrate with a thin layer (∼150 nm) of the adhesive. This substrate was supported on a silicon wafer segment (∼5 mm × 5 mm) connected to a load cell. A microscope objective integrated with the vertical stage and attached to its own secondary lateral translation axes allowed visual evaluation of the contact and retraction events.

Transfer Printing. A PDMS stamp with posts (100 × 100 μm and heights of 100 μm) was positioned above devices or materials structures on a source substrate to allow their retreival and subsequent delivery to a substrate of interest. The printing was performed either with a modified mask aligner (Karl Suss, MJB3) or an automated printing machine shown in Supporting Information Figure SI1.

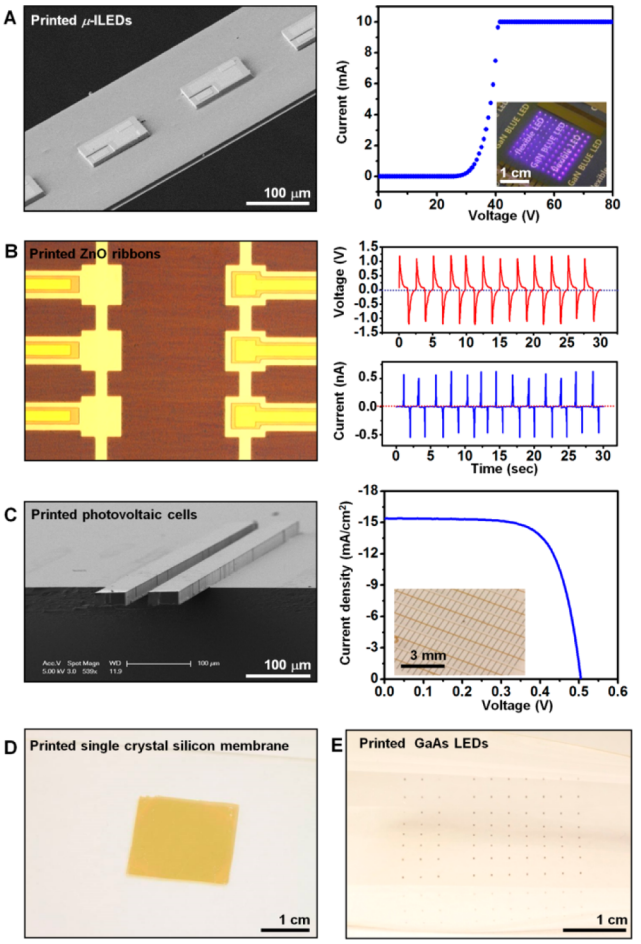

Figure 5. Diverse applications of printed materials in flexible electronics. (A) Tilted SEM image of several 100 × 100 μm^2 μ-ILEDs printed on a adhesive coated 2.5 μm thick plastic sheet and voltage−current (*V*−*I*) characteristic of a square array (10 × 10) of 100 × 100 μm^2 μ-ILEDs printed on an adhesive coated glass plate. The inset shows the array. (B) Optical microscopic image of ZnO mechanical energy harvesters and their electrical properties. Image of a device printed on an adhesive coated 1.2 μm thick film of polyimide, each with a capacitor type geometry. The layer of ZnO (500 nm) lies between bottom (200 nm) and top electrodes (200 nm) of Au that define an active area of 50 μm × 2 mm. A harvester consists of six groups of devices; each group includes 10 separate capacitor structures electrically connected in parallel. The six groups are connected in series. The graphs on the right show the open voltage and short current values of a harvester. (C) Tilted SEM image of two silicon bars printed onto an adhesive coated glass substrate. Bars having lengths of ∼1.55 mm, widths of ∼50 μm, and thicknesses of ∼15−20 μm are transferred individually. The graph on the right shows the measured current density as a function of voltage for a single microscale solar cell. The efficiency and the fill factors of the cell, without any light trapping schemes, are 6.2% and 71%, respectively. The inset shows silicon bar arrays. (D) Photograph of a printed 320 nm thick single crystal silicon membrane, with lateral dimensions of 2 × 2 cm^2, on a glass substrate. (E) GaAs chips with lateral dimensions of 100 × 100 μm^2 printed onto glass.

Fabrication of μ-ILEDs. InGaN (Cermet Inc.) epitaxially grown on sapphire was used as the active material. The epitaxial layers consisted of undoped GaN (3.8 μm), n-type doped GaN (2 μm), multiple quantum wells (0.14 μm), and p-type doped GaN (0.2 μm). After sputter deposition (AJA, ATC 2000) of a bilayer of Ni (15 nm) and Au (15 nm) as a thin p-contact, photolithography and wet etching formed patterned L-shaped current spreading layers. Chlorine based

dx.doi.org/10.1021/cm501002b | *Chem. Mater.* 2014, 26, 3502−3507

inductively coupled reactive ion etching (ICP-RIE; PlasmaTherm, SLR-770) defined square ($40 \times 40\ \mu m^2$) recessed regions to expose the n-type layers. Contact pads to the n- and p- regions, each $25 \times 25\ \mu m^2$, were formed by electron beam evaporation (Temescal, FC-1800) of Cr/Au (15 nm/300 nm). Negative tone photoresist (PR, 7 μm thick; MicroChemicals Inc., AZ nLOF 2070) served as an etch mask to define μ-ILEDs with lateral dimensions of 100 μm × 100 μm.

Fabrication of ZnO Mechanical Energy Harvesters. A series of steps yielded ZnO ribbons in capacitor type geometries for mechanical energy harvesting. A bilayer of Au/Cr (200 nm/10 nm; electron beam evaporation) served as bottom electrodes on a silicon wafer with a 600 nm thick layer of SiO_2 on its surface. Deposition of ZnO (500 nm) was performed using RF magnetron sputtering (AJA) with a deposition rate of ∼150 nm/h, from a ZnO target (99.99%) at a base pressure of 2×10^{-6} Torr and working pressure of 15 mTorr, maintained with a mix of Ar (99.99%):O_2 = 2:1 (sccm). The sputtering occurred at room temperature (RT) with an RF power of 250 W. The top electrodes were formed using methods similar to those for the bottom electrodes. Photolithography defined the top electrode areas (50 μm × 2 mm) for each ZnO ribbon. ZnO ribbons with an area of 100 μm × 2.02 mm resulted from wet chemical etching with HCl (hydrochloric acid):HNO_3 (nitric acid):H_2O (DI water) = 1:1:100 with an etching rate of 200 nm/s through a hard-baked mask of photoresist (AZ4620, Clariant). The baking involved 80 °C for 5 min, 110 °C for 30 min, and then 80 °C for 5 min. Bottom electrodes with areas of 140 μm × 2.02 mm were patterned, using processes similar to those for the top electrodes. The ZnO ribbons were protected by photoresist during partial removal of the SiO_2 with dilute HF (hydrofluoric acid) (DI water: 49% HF = 1:3). The photoresist was removed using a hot acetone spray for 10 s. The ZnO ribbons were retrieved by contacting and then peeling away a PDMS stamp from the Si wafer. Transfer used a film of the adhesive reported here (1500 rpm for 30 s). A spin-cast layer of this same adhesive, hard baked at 110 °C for 3 min, served as encapsulation. Connection lines were obtained by depositing Au/Cr (200 nm/10 nm) by electron beam evaporation. Details appear elsewhere.[25]

Measurement of ZnO Mechanical Energy Harvesters. A semiconductor parameter analyzer (4155C, Agilent) was used to measurement. Corresponding open circuit voltage and short circuit current outputs under mechanical cycling are in Figure 5B. A computer controlled mechanical stage enabled accurate evaluation of properties under bending. The system included a high precision linear stage (ATS100-150; Aerotech, Inc.; U.S.A.), equipped with precision ground ball screw, noncontact rotary encoder with 1000 line/rev, and brushless servomotor to achieve a motion with an accuracy of ±0.5 μm and a bidirectional repeatability of ±0.3 μm over 150 mm stage motion range. The stage can achieve velocities up to 100 mm/s with maximum side load of 100 N in horizontal configuration. The stage motion was controlled with a Soloist single axis PWM digital controller (SOLOISTCP20; Aerotech, Inc.; U.S.A.) and USB interface. Additionally, two U-Form Vise grips (TH240k, Grip Engineering Thümler GmbH; Germany) were attached to the stage. Pyramid shape jaws (TH240k-BP, Grip Engineering Thümler GmbH; Germany) were connected to the vices to achieve maximum tensile gripping force of 2.5 kN of the specimen during the test. A LabVIEW (National Instruments Corporation; U.S.A.) based program was designed to control the stage to perform the test cycle. Details appear elsewhere.[26]

Fabrication of Silicon Bars and Microscale Solar Cells. The fabrication of bars of silicon with thicknesses between 15 and 20 μm began with a P-type Czochralski Si ⟨111⟩ wafers (1−10 Ω·cm, 450 μm thickness, Virginia Semiconductor). A layer of SiO_2 (600 nm) formed by plasma enhanced vapor deposition (PlasmaTherm SRL) and patterned photolithographically served as an etch mask for defining trenches to a depth of 15−20 μm in the exposed regions of the silicon, using inductively coupled plasma reactive ionic etcher (STS ICP-RIE). Solid state doping of boron and phosphorus at 1000 °C and 950 °C, respectively, for 30 min (Boron, BN-1250, Saint Gobain) and 10 min (Phosphorus, PH-1000N, Saint Gobain) produced a rectifying P−N junction. Deposition of conformal bilayers of SiO_2/Si_3N_4 on both the sidewalls and the top surface and annealing at 400 °C for 30 min protected the top surface of the silicon wafer. Protection of top and sidewalls by deposition of Cr/Au layers using e-beam evaporator (Tumescal, FC 1800) enabled etching the trench region of the dielectric layer selectively by RIE. KOH (PSE-200, Transene) etching releases through the trenches in the Si ⟨110⟩ directions much faster than the other orientations of silicon. Release yield of ∼99% was achieved from the host wafers. Boron doping with a SiO_2/Si_3N_4 mask at the bottom region completed the μ-cells. Arrays of μ-cells with PDMS (Sylgard 184 Silicone Elastomer Kit) anchors at their ends can be selectively released and printed onto adhesive-coated foreign substrates.

Fabrication for MIM Capacitor. The processing began with uniform deposition of metal (Cr/Au = 10/400 nm) on a high-resistivity (∼8000 Ω) (111) bulk wafer with 830 nm of thermally grown SiO_2 to reduce substrate coupling and RF losses. Formation of a layer of the adhesive involved spin-coating at 1500 rpm for 30 s (820 nm), exposure to UV, and then hard baking. The top metal (Cr/Au = 10/500 nm) was deposited directly on the cured adhesive. Photolithography defined the geometry of this metal, which also served as a mask to pattern the adhesive by reactive ion etching (Unaxis 790). The bottom metal was also patterned using phtolithography and wet etching. A thick layer of SU-8 resist defined via holes and isolation for the top and bottom electrodes. Metal deposition and lift off defined ground−signal−ground (GSG) pads for RF probing.

Characterization of Electrical, Optical, and Thermal Properties. A semiconductor parameter analyzer (4155C, Agilent) was used to measure the electrical properties.

■ ASSOCIATED CONTENT

Ⓢ Supporting Information

Additional details of experimental results. This material is available free of charge via the Internet at http://pubs.acs.org.

■ AUTHOR INFORMATION

Corresponding Authors

*E-mail: taeilkim@skku.edu (T.-i.K.).
*E-mail: jrogers@uiuc.edu (J.A.R.).

Notes

The authors declare no competing financial interest.

■ ACKNOWLEDGMENTS

The authors would like to thank Dr. Rak-Hwan Kim (Samsung), Il-Sun Song (UIUC), and Dr. Yongho Kim (SKKU) for the assistance in fabrication of GaAs LED chips, transfer printing, and helpful discussion for FT-IR results. This work was supported by Basic Science Research Program through the National Research Foundation of Korea Grant funded by the Ministry of Science, ICT & Future Planning (2009-0083540), and NRF-2013-R1A1A1061403 in Korea. The work on materials and transfer printing was supported by Office of Naval Research under grant N00014-10-1-0989.

■ REFERENCES

(1) Lee, C. H.; Kim, D. R.; Zheng, X. *Proc. Natl. Acad. Sci. U.S.A.* **2010**, *107*, 9950.

(2) Fan, Z.; Ho, J. C.; Takahashi, T.; Yerushalmi, R.; Takei, K.; Ford, A. C.; Chueh, Y.-L.; Javey, A. *Adv. Mater.* **2009**, *21*, 3730.

(3) Kim, D.-H.; Ahn, J.-H.; Choi, W.-M.; Kim, H.-S.; Kim, T.-H.; Song, J.; Huang, Y. Y.; Zhuangjjan, L.; Chun, L.; Rogers, J. A. *Science* **2008**, *320*, 570.

(4) Yang, H.; Zhao, D.; Chuwongin, S.; Seo, J.-H.; Yang, W.; Shuai, Y.; Berggren, J.; Hammar, M.; Ma, Z.; Zhou, W. *Nat. Photonics* **2012**, *6*, 617.

(5) Ghaffari, A.; Hosseini, A.; Xu, X.; Kwong, D.; Subbaraman, H.; Chen, R. T. *Opt. Express* **2010**, *18*, 20086.
(6) Sum, L.; Qin, G.; Seo, J.-H.; Celler, G. K.; Zhou, W.; Ma, Z. *Small* **2010**, *6*, 2553.
(7) Hammock, M. L.; Chortos, A.; Tee, B.C.-K.; Tok, J.B.-H.; Bao, Z. *Adv. Mater.* **2013**, *25*, 5997.
(8) Kim, T.-I.; McCall, J. G.; Jung, Y. H.; Huang, X.; Siuda, E. R.; Li, Y.; Song, J.; Song, Y. M.; An Pao, H.; Kim, R.-H.; Lu, C.; Lee, S. D.; Song, I.-S.; Shin, G.; Al-Hasani, R.; Kim, S.; Tan, M. P.; Huang, Y.; Omenetto, F. G.; Rogers, J. A.; Bruchas, M. R. *Science* **2013**, *240*, 211.
(9) Hwang, S.-W.; Tao, H.; Kim, D.-H.; Cheng, H.; Song, J.-K.; Rill, E.; Brenckle, M. A.; Panilaitis, B.; Won, S. M.; Kim, Y.-S.; Song, Y. M.; Yu, K. J.; Ameen, A.; Li, R.; Su, Y.; Yang, M.; Kaplan, D. L.; Zakin, M. R.; Slepian, M. J.; Huang, Y.; Omenetto, F. G.; Rogers, J. A. *Science* **2012**, *337*, 1640.
(10) Kim, B.-S; Lee, S. W.; Yoon, H.; Strano, M. S.; Shao-Horn, Y.; Hammond, P. T. *Chem. Mater.* **2010**, *22*, 4791.
(11) Ko, H.; Jiang, C.; Tsukruk, V. V. *Chem. Mater.* **2005**, *17*, 5489.
(12) Kim, S.; Wu, J.; Carlson, A.; Jin, S. H.; Kovalsky, A.; Glass, P.; Liu, Z.; Ahmed, N.; Elgan, S. L.; Chen, W.; Ferreira, P. M.; Sitti, M.; Huang, Y.; Rogers, J. A. *Proc. Natl. Acad. Sci. U.S.A.* **2010**, *107*, 17095.
(13) Carlson, A.; Bowen, A. M.; Huang, Y.; Nuzzo, R. G.; Rogers, J. A. *Adv. Mater.* **2012**, *24*, 5284.
(14) (a) Bower, C. A.; Menard, E.; Bonafede, S.; Burroughs, S. *Proceedings of the Electronic Components and Technology Conference (59th ECTC)*, San Diego, CA; IEEE: 2009, p *618*. (b) Hamer, J.; Cok, R.; Parrett, G.; Winters, D.; Bower, C.; Menard, E.; Bonafede, S. *SID 2009 Digest* **2009**, *15*, 947.
(15) Keum, H.; Chung, H.; Kim, S. *ACS Appl. Mater. Interfaces* **2013**, *5*, 6061.
(16) Carlson, A.; Kim-Lee, H.-J.; Wu, J.; Elvikis, P.; Cheng, H.; Kovalsky, A.; Elgan, S.; Yu, Q.; Ferreira, P. M.; Huang, Y. G.; Turner, K. T.; Rogers, J. A. *Appl. Phys. Lett.* **2011**, *98*, 264104.
(17) Kim, C.; Burrows, P. E.; Forrest, S. R. *Science* **2000**, *288*, 831.
(18) Xia, Y.; Whitesides, G. M. *Angew. Chem., Int. Ed.* **1998**, *37*, 551.
(19) Crespo-Biel, O.; Dordi, B.; Maury, P.; Peter, M.; Reinhoudt, D. N.; Hukens, J. *Chem. Mater.* **2006**, *18*, 2545.
(20) Loo, Y.-L.; Willett, R. L.; Baldwin, K. W.; Rogers, J. A. *J. Am. Chem. Soc.* **2002**, *124*, 7654.
(21) Kim, T.-I; Jung, Y. H.; Song, J.; Kim, D.; Li, Y.; Kim, H.-S.; Song, J. J.; Wierer, I.-S.; Pao, H. A.; Huang, Y.; Rogers, J. A. *Small* **2012**, *8*, 1643.
(22) Kim, T.-I.; Jung, Y. H.; Chung, H.-J.; Yu, K. J.; Ahmed, N.; Corcoran, C.; Park, J. S.; Jin, S. H.; Rogers, J. A. *Appl. Phys. Lett.* **2013**, *102*, 182104.
(23) http://www.filmtronics.com/sog/sogtable.html (accessed March 4, 2014).
(24) Breschi, M.; Fabiani, D.; Sandrolini, L.; Colonna, M.; Sisti, L.; Vannini, M.; Mazzoni, A.; Ruggeri, A.; Pashley, D. H. *Dent. Mater.* **2012**, *28*, 1024.
(25) Dagdeviren, C.; Hwang, S.-W.; Su, Y.; Kim, S.; Cheng, H.; Gur, O.; Haney, R.; Omenetto, F. G.; Huang, Y.; Rogers, J. A. *Small* **2013**, *9*, 3398.
(26) Dagdeviren, C.; Yang, B. D.; Su, Y.; Tran, P. L.; Joe, P.; Anderson, E.; Xia, J.; Doraiswamy, V.; Dehdashti, B.; Feng, X.; Lu, B.; Poston, R.; Khalpey, Z.; Ghaffari, R.; Huang, Y.; Slepian, M. J.; Rogers, J. A. *Proc. Natl. Acad. Sci. U.S.A.* **2014**, *111*, 1927.